11-5-2008

Geocoronal Hydrogen Observations Spanning Three Solar Minima

S. M. Nossal
University of Wisconsin - Madison

E. J. Mierkiewicz
University of Wisconsin - Madison, mierkiee@erau.edu

F. L. Roesler
University of Wisconsin - Madison

L. M. Haffner
University of Wisconsin - Madison

R. J. Reynolds
University of Wisconsin - Madison

See next page for additional authors

Scholarly Commons Citation

Nossal, S. M., Mierkiewicz, E. J., Roesler, F. L., Haffner, L. M., Reynolds, R. J., & Woodward, R. C. (2008). Geocoronal Hydrogen Observations Spanning Three Solar Minima. *Journal of Geophysical Research, 113*(A11307). https://doi.org/10.1029/2008JA013380

Geocoronal hydrogen observations spanning three solar minima

S. M. Nossal,[1] E. J. Mierkiewicz,[1] F. L. Roesler,[1] L. M. Haffner,[2]
R. J. Reynolds,[2] and R. C. Woodward[3]

Received 12 May 2008; revised 31 July 2008; accepted 14 August 2008; published 5 November 2008.

[1] The 11-year solar cycle is a dominant source of natural variability in the upper atmosphere, and its effect on atomic hydrogen distributions and emissions must be understood to investigate possible signs of longer-term climatic trends in this region. We present midlatitude geocoronal hydrogen Balmer α observations from solar cycle 23 (1997–2006) and three solar minimum periods, 1985, 1997, and 2006. The 1997 through 2006 observations were taken with the Wisconsin H-α Mapper Fabry-Perot (WHAM), a ground-based CCD-annular summing instrument that began observations at the Kitt Peak Observatory in Arizona in 1997. The 1985 observations were made with a similarly designed "pre-WHAM" Fabry-Perot Interferometer utilizing photomultiplier detection and located in Wisconsin. WHAM has consistently observed higher column emission intensities during solar maximum periods than during solar minimum conditions, with the ratio dependent upon the viewing geometry. The observations from three solar minimum periods agree to within 18% uncertainties over most of the shadow altitude range. An analysis of recent Fabry-Perot observations of upper atmospheric hydrogen during solar cycle 23 and during three solar minima (1985, 1997, 2006) established a reference data set of highly precise, consistently calibrated, thermospheric plus exospheric hydrogen column emission observations from northern midlatitudes that can be used to compare with future observations.

Citation: Nossal, S. M., E. J. Mierkiewicz, F. L. Roesler, L. M. Haffner, R. J. Reynolds, and R. C. Woodward (2008), Geocoronal hydrogen observations spanning three solar minima, *J. Geophys. Res.*, *113*, A11307, doi:10.1029/2008JA013380.

1. Introduction

[2] The investigation of natural variation and climate change in the upper atmosphere requires long-term data sets. Knowledge of the middle and upper atmosphere in concert with information about the lower atmosphere is becoming increasingly recognized as important for understanding the atmospheric climate system as a whole [*Roble and Dickinson*, 1989; *Roble*, 1995; *Garcia et al.*, 2007]. Understanding the influence of sources of natural variability, such as the solar cycle, is needed to characterize the thermosphere and exosphere, to understand coupling processes between atmospheric regions, and to isolate signatures of human-caused change. One of the potential diagnostics of global change in the upper atmosphere is exospheric hydrogen, which is predicted to rise in concentration in response to increases in tropospheric methane, a primary greenhouse gas.

[3] The exosphere is a unique region of the atmosphere characterized by low densities, long mean free paths, and non-Maxwellian orbital dynamics including escape trajectories (see, for example, *Chamberlin and Hunten* [1987]). Geocoronal hydrogen primarily results from lower and middle atmospheric chemistry involving radiatively important species such as water vapor and methane, as well as molecular hydrogen. Hydrogen in the geocorona is the byproduct of middle and upper atmospheric chemical, photolysis, and charge exchange reactions involving hydrogenous species such as H_2O, CH_4, H_2, OH, and CH_2O [*Brasseur and Solomon*, 2005]. Neutral hydrogen interacts with the ionosphere through charge exchange reactions with O^+ and H^+ [*Chamberlin and Hunten*, 1987]. Atomic hydrogen spans the thermosphere and exosphere, becoming increasingly dominant with altitude. Because of its long orbital trajectories, geocoronal hydrogen is more globally mixed compared with hydrogenous species below, and thus constitutes a measurement more representative of a global average.

[4] Hydrogen-containing species in the middle and upper atmosphere are predicted to increase along with increases in methane, a primary greenhouse gas. The methane abundance in 2005 of about 1774 ppb is more than double its pre-industrial value, with growth rates in the late 1970s and early 1980s of about 1% yr^{-1} [*Solomon et al.*, 2007]. The growth rate of methane has significantly decreased since the early 1990s and was close to zero for the period from 1999 to 2005 [*Solomon et al.*, 2007]. High interannual variability

[1]Department of Physics, University of Wisconsin-Madison, Madison, Wisconsin, USA.
[2]Department of Astronomy, University of Wisconsin-Madison, Madison, Wisconsin, USA.
[3]Department of Computer Science, Engineering, Physics and Astronomy, University of Wisconsin-Fond du Lac, Fond du Lac, Wisconsin, USA.

0148-0227/08/2008JA013380

has been observed in the methane growth rate that has not been fully explained [*Solomon et al.*, 2007].

[5] Using the National Center for Atmospheric Research (NCAR) global mean model of the mesosphere, thermosphere, and ionosphere, *Roble and Dickinson* [1989] provided seminal insights regarding the sensitivity of the middle and upper atmospheric total density, composition and temperature to a doubling of the atmospheric concentrations of carbon dioxide and methane, the two most important anthropogenic greenhouse gases. Hydrogen at upper thermospheric altitudes was predicted by the global mean model to increase by about 40–50% in response to a doubling of tropospheric warming gases, principally methane [*Roble and Dickinson*, 1989], consistent with calculated projections by *Ehhalt* [1986]. Recent modeling with the Thermosphere Ionosphere Mesosphere Electrodynamics General Circulation Model (TIME-GCM) [for model description, see *Roble and Ridley*, 1994] projects on the order of 75% increases in upper thermospheric hydrogen in response to a doubling of methane and carbon dioxide during solar medium conditions (R. G. Roble, personal communication, 2008). The TIME-GCM contains updated cooling rates and odd-nitrogen chemistry not included in the version of the NCAR global mean model used by *Roble and Dickinson* [1989] in their climatic study using the global mean model with equilibrium greenhouse gas doubling conditions.

[6] University of Wisconsin observers have compiled a record of geocoronal hydrogen column emission observations taken with ground-based Fabry-Perot Interferometers from northern midlatitudes spanning three solar cycles. Ground-based remote sensing via Fabry-Perot observations of the fluorescent Balmer-α emission from atomic hydrogen is one of the primary methods for studying hydrogen in the upper thermosphere and exosphere. This emission arises primarily from solar excitation of the hydrogen atom by the line center of the solar Lyman β flux. The resulting Balmer α emission intensity is a measurement of the column of emissions along the observational line-of-sight, with the peak in the emission arising from just above the Earth's shadow. Wisconsin observers have made observations of the hydrogen Balmer α emission from mid latitudes since 1977 (see, for example, *Yelle and Roesler* [1985], *Shih et al.* [1985], *Nossal et al.* [1993, 2004, 2006], *Bishop et al.* [2001], *Mierkiewicz* [2002], and *Mierkiewicz et al.* [2006, and references therein]). These data were taken primarily from the Stoughton and Pine Bluff, Wisconsin, observatories during solar cycles 21 and 22 and from Kitt Peak, Arizona and Pine Bluff, Wisconsin, during solar cycle 23.

[7] This paper describes solar minimum observations during three solar minima, 1985, 1997, and 2006. We also include solar cycle observations taken during different phases of solar cycle 23 with the Wisconsin H-α Mapper Fabry-Perot (WHAM). Emphasis has been placed on calibration and data quality issues to facilitate inter-annual investigations and to establish baseline data sets for future data comparisons.

2. Observations

[8] Wisconsin observers have been making ground-based Fabry-Perot observations of the geocoronal Balmer α column emission from midlatitudes since 1977, with some gaps in the observational record. Throughout this period, many of the observations were specifically designed for geocoronal studies and others were the terrestrial spectra present in astronomical observations made for studies of the interstellar medium and comets. All of the observations were made using double etalon Fabry-Perot instruments. The solar cycle 21 and 22 observations were made from Wisconsin using photomultiplier detection, while the solar cycle 23 observations have been made using similarly designed Fabry-Perot instruments coupled to CCD detectors located at the Kitt Peak, Arizona and Pine Bluff, Wisconsin observatories. All of the observations were calibrated using nebular calibration sources tied to the North American Nebula.

[9] Multiyear comparisons of upper atmospheric Balmer α emissions require cross-calibrated instrumentation, a stable calibration source, reproducible observing conditions, separation of the terrestrial from the Galactic emission line, and consistent data analysis accounting for differences in viewing geometry. Our strategies for achieving these requirements are summarized below and explained in more detail by *Nossal et al.* [2006] and *Mierkiewicz et al.* [2006]. The first of these companion papers discusses the technique of Fabry-Perot spectroscopy applied to geocoronal hydrogen studies, including strategies for obtaining data of sufficient precision for studies of the geocoronal line profile, retrieval of the hydrogen column abundance, and long-term data comparisons [*Mierkiewicz et al.*, 2006]. The second paper highlights aspects of instrumental, observational, and data reduction procedures important for the acquisition, analysis, and interpretation of long-term geocoronal hydrogen emission data sets [*Nossal et al.*, 2006].

[10] The observations included in this paper were taken with the remotely operable Wisconsin H-α Mapper Fabry-Perot (WHAM) when it was located at Kitt Peak Observatory, near Tuscon, Arizona (31.98°N; 248.40°E), and with an earlier "pre-WHAM" Fabry-Perot, then located at the Wisconsin Pine Bluff Observatory (43.07°N; 270.33°E). In addition to WHAM, Wisconsin currently operates a second annular summing Fabry-Perot interferometer. The latter instrument is located at Pine Bluff, and is also used for observations of geocoronal hydrogen emissions (see Figure 1 and *Mierkiewicz et al.* [2006]). Fabry-Perot spectrometers combine the advantages of high spectral resolution with high throughput, thus being well suited for observations of faint airglow emissions, such as those from geocoronal hydrogen ($\sim$1–15 Rayleighs) [*Roesler*, 1974].

[11] Both WHAM and the Fabry-Perot located at the Pine Bluff, Wisconsin, Observatory employ the annular summing spectroscopy technique. Both instruments are pressure-tuned, large aperture (15 cm), double etalon Fabry-Perot spectrometers using a cryogenically cooled, high quantum efficiency Charge Coupled Device camera [*Mierkiewicz et al.*, 2006]. In annular summing spectroscopy, the Fabry-Perot's annular interference pattern is imaged onto the CCD, thereby collecting light simultaneously in all spectral elements over the observed spectral range [*Reynolds et al.*, 1990; *Coakley et al.*, 1996], increasing the signal-to-noise of the observations.

[12] Each instrument is coupled to a pointing and tracking siderostat, enabling observations to avoid regions of bright

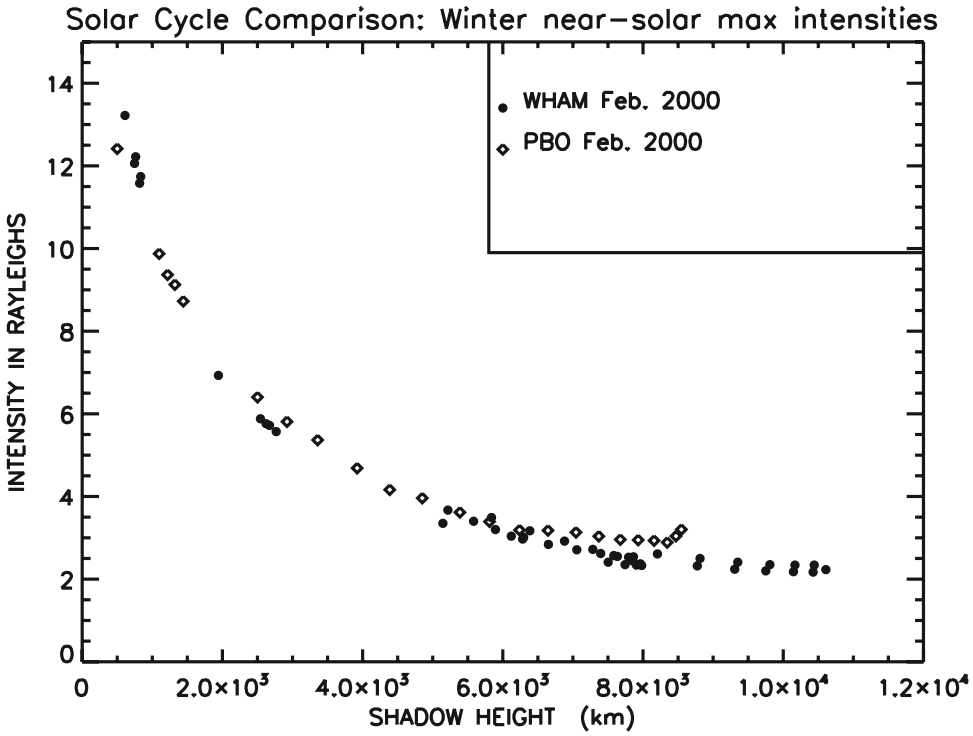

Figure 1. Balmer α column emission observations from the WHAM Fabry-Perot at the Kitt Peak, Arizona Observatory and from the Pine Bluff, Wisconsin Observatory taken during the same dark of the moon period in February 2000.

Galactic emission and to select regions of large Doppler shift between the terrestrial and Galactic emission lines. The pointing capability also facilitates making observations in multiple viewing geometries and observations of nebular calibration sources for relative and absolute flux calibration.

[13] The Wisconsin H-α Mapper (WHAM) Fabry-Perot is a remotely operable instrument with resolution ($R = \lambda/\Delta\lambda \approx 25{,}000$) sufficient for retrieval of the Balmer α column emission intensity and for separation of the geocoronal line from the Doppler-shifted Galactic line. The higher resolution Pine Bluff Observatory (PBO) Fabry-Perot is of sufficient resolution to ($R \approx 80{,}000$) to retrieve the geocoronal Balmer α line profile as well as the column emission intensity. The etalons for both instruments are made of fused silica with highly reflective (91 ± 1% near Balmer α) broadband (4500−9000 Angstrom) coatings [*Mierkiewicz et al.*, 2006; *Trauger*, 1976]. WHAM's resolving etalon has a fixed gap spacing of $l = 0.0471$ cm, and its lower resolution etalon has a gap of and $l = 0.0201$ cm. The Pine Bluff Fabry-Perot has a gap of $l = 0.149$ cm for the resolving etalon and $l = 0.0524$ cm for the lower resolution etalon (for further discussion, see *Mierkiewicz et al.* [2006]). The lower resolution etalon extends the free spectral range of the resolving etalon by blocking unwanted multiple orders of interference, thereby enhancing the contrast between the peak and the background of the instrumental profile, suppressing ghost emissions, and reducing parasitic light contamination.

[14] WHAM is funded by the Astronomy Division of the National Science Foundation (NSF-AST0607512) to make an all-sky survey of interstellar medium emissions. One of WHAM's major astronomical accomplishments is the completion of a Northern hemisphere all-sky survey of the velocity-resolved interstellar Balmer α emission intensity [*Haffner et al.*, 2003; *Reynolds*, 1997]. Dedicated WHAM geocoronal observations and the terrestrial emissions present in the WHAM astronomical spectra offer a rich resource for studying the geocorona [*Mierkiewicz et al.*, 2006; *Nossal et al.*, 2001, 2004, 2006]. The WHAM instrument has been operated since 1997 from the Kitt Peak Observatory in Tucson, Arizona and completed observations at this site in March of 2008.

[15] In order to complete its astronomical mission of mapping the interstellar medium, WHAM must move to the Southern Hemisphere and will soon be transported to the Cerro Tololo Inter-American Observatory, North of Santiago, Chile. The Fabry-Perot located at the Pine Bluff, Wisconsin, Observatory will continue to extend the long-term baseline of northern midlatitude geocoronal hydrogen observations. Previous comparisons (see Figure 1) indicate a high correlation between observations taken by WHAM from Kitt Peak, Arizona, and by the high-resolution Fabry-Perot at Pine Bluff, Wisconsin, during the same observing period [*Mierkiewicz*, 2002; *Nossal et al.*, 2006].

[16] The 1985 solar minimum observations were made with the "pre-WHAM" Fabry-Perot, located then at the Pine Bluff Observatory [*Reynolds*, 1984]. This instrument was coupled to a pointing and tracking siderostat. The pre-WHAM instrument used the same etalons, coatings, and spacers (R∼25,000) as in the present WHAM instrument, but was coupled to a cryogenically cooled photomultiplier, rather than to a CCD camera. The pre-WHAM used pressure scanning to obtain a spectral profile with the photomultiplier as a photon counter.

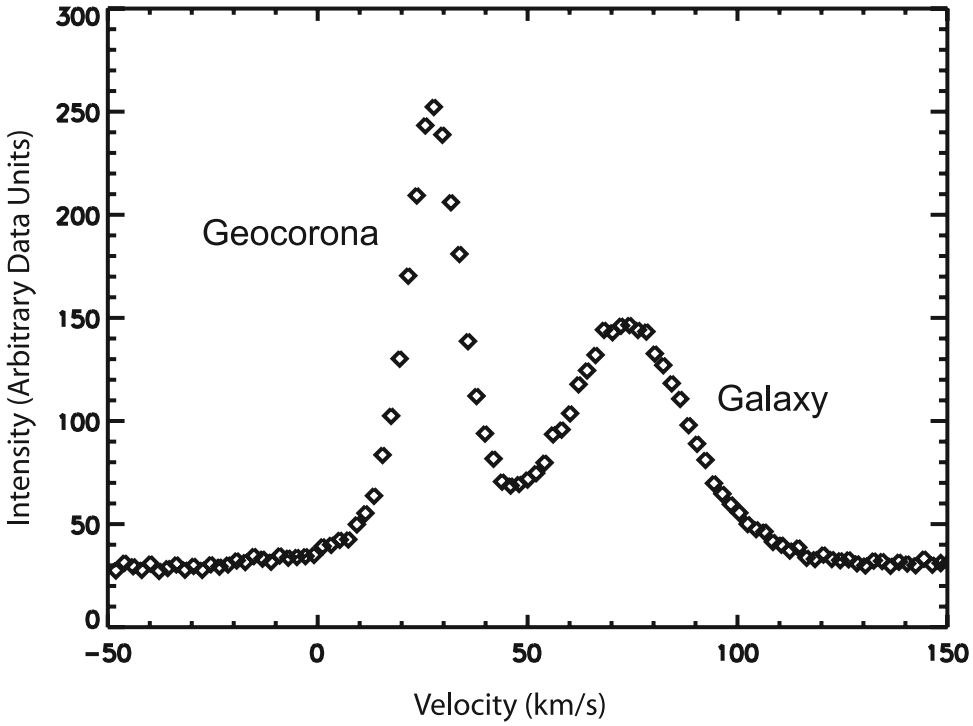

Figure 2a. Sample geocoronal emission spectra taken with the Wisconsin H-α Mapper Fabry-Perot. Spectral displacement is expressed in velocity units with the "zero" velocity placed at an arbitrary location. (a) This observational direction contains both the geocoronal emission (tall narrow peak) and the Galactic emission (broader emission).

[17] The field of view on the sky of the WHAM instrument is 1.0°, of the annular-summing Pine Bluff Fabry-Perot is ~1.4°, and of the pre-WHAM instrument was 0.8°. The absolute intensity calibration for each instrument was performed through comparisons with nebular observations taken by the same instrument with the same field of view.

3. Data Analysis

[18] We have focused our analysis on observations with the highest levels of data quality to facilitate multiyear comparisons and to avoid misinterpretation of artifacts. Our observations are taken under moonless conditions, to avoid scattered moonlight interference, and during clear sky conditions because even high, thin cirrus clouds can produce attenuation and scattering from regions outside the field of view.

[19] A two component model accounting for the two Balmer α fine structure components excited directly by solar Lyman β radiation ($3^2P_{3/2} \rightarrow 2^2S_{1/2}$ and $3^2P_{1/2} \rightarrow 2^2S_{1/2}$) was convolved with the instrumental profile and fit to the observational spectra [*Nossal et al.*, 2006; *Mierkiewicz et al.*, 2006] using the *Voigt-fit* spectral fitting code developed by *Woodward*. These directly excited fine structure components occur in a 2:1 ratio. The combined area of the fine structure components is then compared with the area of the nebular spectrum to calculate the geocoronal intensity, adjusting for differences in atmospheric extinction due to differences in slant path between the directions of the geocoronal and nebular observations (see section 4). The *Voigt-fit* spectral fitting code enables Gaussian parameters to be linked, fixed, or free, thereby facilitating modeling of the atomic physics, as well as the fitting of the continuum background.

[20] The high signal-to-noise WHAM observations have enabled us to understand with greater clarity, observational and analysis factors that impact the accuracy of the retrieved geocoronal intensity. In particular, Galactic emission, which can be of comparable magnitude or greater than that of the geocorona, must be carefully accounted for (see Figure 2a). Here the geocoronal emission is the tall narrow peak and the Galactic emission is the broader peak. The spectral displacement is expressed in velocity units with an arbitrary "zero" velocity. Isolation of the terrestrial emission therefore requires an accurate accounting of the Galactic emission. WHAM has sufficient resolution to isolate the geocoronal from the Galactic emission, except in cases of major overlap between the two emissions. The WHAM Galactic survey map [*Haffner et al.*, 2003] (http://www.astro.wisc.edu/wham/survey) provides information about the intensity, structure, and Doppler shift of the Galactic emission in a given observational look direction and facilitates the planning of geocoronal observations in low Galactic emission directions and removal of the Galactic background.

[21] For the WHAM portion of the solar cycle study we have chosen to include only observations pointed toward very low Galactic emission regions of the sky so as to minimize uncertainty due to the presence of Galactic emission in the spectra. These regions include the Lockman Window region and typically have Galactic intensities of

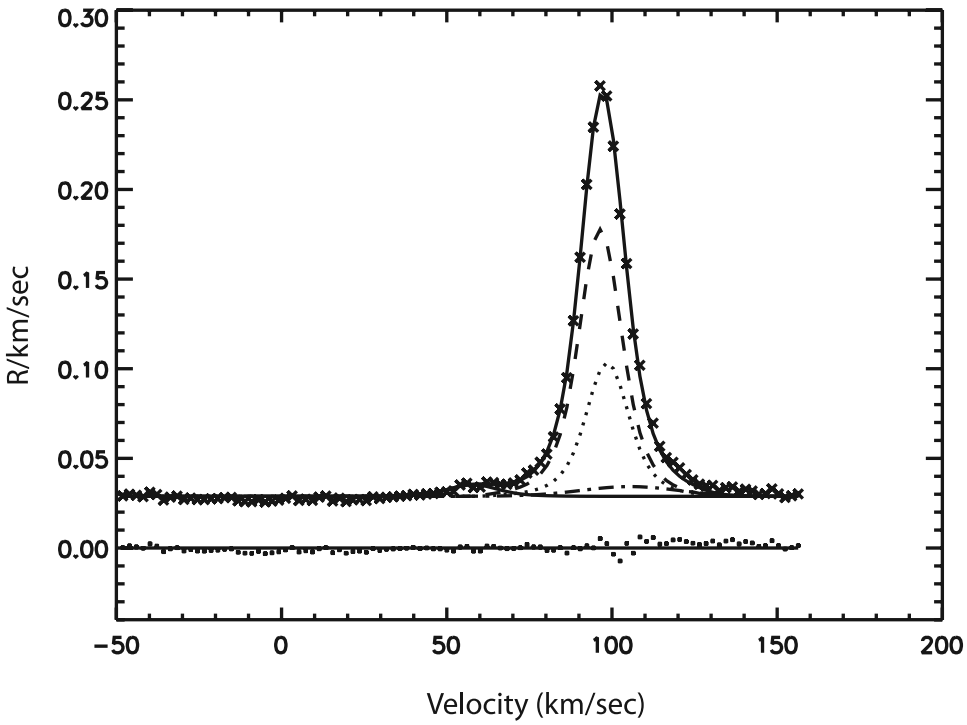

Figure 2b. Observation pointed toward a region of low Galactic emission (30-second exposure). In relation to the arbitrary zero point, the centroid of the two component fit to the geocoronal line is located at 96.8 km/s, and its intensity is 4.1 Rayleighs. The fit also includes the Galactic emission (0.20 Rayleighs) at 105 km/s and a faint O_2 band atmospheric emission (0.13 Rayleighs) at 57.7 km/s [*Nossal et al.,* 2004; *Hausen et al.*, 2002]. The WHAM solar cycle study includes only observations pointed toward low Galactic emission regions so as to minimize uncertainty due to the Galactic emission.

0.3 Rayleighs or less at Balmer α [*Hausen et al.*, 2002]. Figure 2b shows an example WHAM spectrum from an observation pointed toward a low Galactic emission region of the sky where the Galactic emission was 0.20 Rayleighs. Also included is a faint O_2 atmospheric band emission [*Nossal et al.*, 2004; *Hausen et al.*, 2002]. This spectrum contains maximum overlap between the Galactic and geocoronal emissions and was used to assess the upper limits in the uncertainty in intensity due to the Galactic emission when it was not explicitly included in the fits to the low Galactic emission region data used in this solar cycle study. We assess this uncertainty as less than 4%. For the spectrum of Figure 2b, the retrieved geocoronal intensity differed by 2.8% when the Galactic emission was not explicitly included.

[22] The shadow altitude is the viewing geometry parameter with the greatest influence on the geocoronal Balmer α column emission intensity (see Figure 3). The shadow altitude is determined by the black level of solar Lyman β radiation (102 km) and the look direction of the observations. The high signal-to-noise of the WHAM data indicate that for a given shadow altitude, differences in zenith angle can produce small, but discernable differences in geocoronal intensity [*Nossal et al.*, 2001]. Observations at high zenith angles are more greatly effected by atmospheric scattering than those close to the zenith. To minimize uncertainty due to atmospheric scattering along longer observational slant paths at high zenith angles, we have only included observations taken at zenith angles of less than 50 degrees for both the 1985 Pine Bluff and the solar cycle 23 WHAM observations included in this solar cycle study. The absolute intensity calibration accounts for differing amounts of atmospheric extinction along different slant paths see equation (1).

[23] We limited the WHAM solar cycle study to observations made during winter months when observing nights are longer with typically better sky conditions than during other times of the year. Observations taken during the same season minimizes potential seasonal effects when comparing observations, and if pointed in the same region of the sky result in reproducible viewing geometries from year to year.

[24] We have also found that small differences in sky condition can produce more scatter in the data. Nights when WHAM observational notes indicated that the skies were clear overhead during the time of observations but that clouds had been sighted earlier or later in the evening often correlated with greater scatter compared with nights that were clear throughout, suggesting that there may have been high cirrus present during the former. We checked the observational notes for the nights corresponding to all of the WHAM observations included in our solar cycle study to strive to insure that the observations were taken under clear sky conditions.

4. Calibration

[25] The absolute intensity of the geocoronal and Galactic H-α column emission intensities are calibrated through

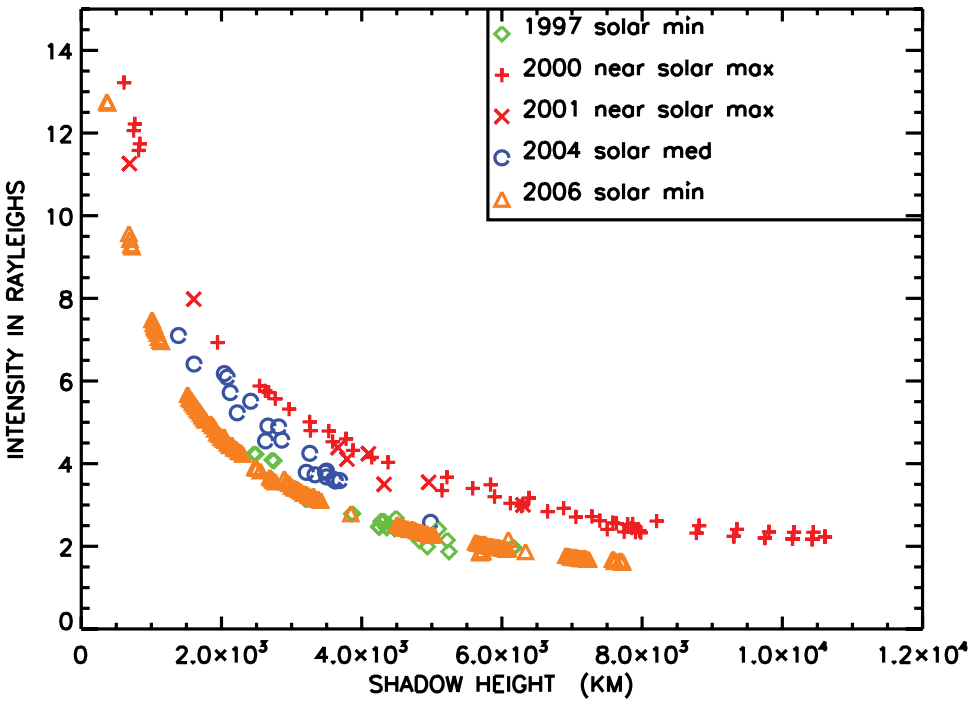

Figure 3. Solar cycle 23 WHAM thermospheric plus exospheric Balmer α column emission intensity observations taken between December and the Spring equinox and in observing directions pointed toward very low Galactic emission regions of the sky. The 1997 solar minimum (F10.7 69–76) data are from 10 nights of observations, the 2000 and 2001 near solar maximum data (F10.7 134–163) are from eight nights of observations, the 2004 solar medium data (F10.7 100–118) are from five nights of observations, and the 2006 solar minimum data (F10.7 75–77) are from two nights of observations. The observations are the primary measurements, uncorrected for tropospheric scattering. An upper boundary on the relative uncertainty associated with comparisons of WHAM observations of the Balmer α column emission intensity toward low Galactic emission regions is ~9.6% (see text).

comparisons with H-α emissions from standard astronomical nebular sources, all of which have been tied to the North American Nebula (NAN). Nebular calibration is internally consistent and is used for calibrating all of the Wisconsin-based atmospheric, planetary, and astronomical hydrogen H-α observations. Nebular calibration offers long-term stability and like the geocorona, nebulae are spatially extended line sources rather than continuum sources. The use of nebular calibration minimizes uncertainty due to atmospheric extinction corrections since both the geocoronal hydrogen and the nebular calibration sources are outside of the Earth's atmosphere. Corrections are made for differences in atmospheric extinction because of differences in slant path. Details about procedures for assessing and correcting for atmospheric extinction can be found in *Mierkiewicz et al.* [2006] and *Nossal et al.* [2006].

[26] The patch of the North American Nebula used for the H-α calibration is centered at 85.60° Galactic longitude and −0.71° Galactic latitude (right ascension 20h 57m 59s and declination +44d 34′ 50″ in J2000 coordinates). The absolute intensity of the NAN observed by the WHAM instrument at Kitt Peak is 800 Rayleighs ± 10%. There is about a 5% uncertainty in the relative calibration due to night-to-night variability in the transmittance of the atmosphere above Kitt Peak.

[27] The intensity of the geocoronal emission can be calculated from the following expression on the basis of the Beer-Lambert Law (equation (1)).

$$I_{geo} = I_{NAN}\left[\frac{A_{geo}}{A_{NAN}}\right]\left[\frac{\exp[-\tau\sec(ZA_{NAN})]}{\exp[-\tau\sec(ZA_{geo})]}\right]\left[\frac{\text{exposure time}(NAN)}{\text{exposure time}(geo)}\right] \quad (1)$$

where

I_{geo}	geocoronal intensity
I_{NAN}	intensity of the North American Nebula (NAN)
A_{geo}	area of the geocoronal emission spectral profile
A_{NAN}	area of the NAN emission spectral profile
τ	atmospheric extinction coefficient
ZA_{geo}	zenith angle of the geocoronal observation
ZA_{NAN}	zenith angle of the NAN observation
exposure time(geo)	exposure time for the geocoronal observation (in sec)
exposure time(NAN)	exposure time for the NAN observation (in sec)

Table 1. WHAM Calibration Factors and the Number of Observations of the North American Nebula used to Calculate Each Year's Calibration Factor

Year	1997	1999–2000	2001	2003–2004	2005–2006
F_{NAN}	25.5	23.2	22.7	22.7	22.3
No. of spectra	11	9	4	5	15

[28] The intensity of the North American Nebula (I_{NAN}) is 800 Rayleighs ± 10% observed by WHAM with a 1.0° field of view, 850 Rayleighs ± 6% observed by the pre-WHAM Fabry-Perot with a 0.8° field of view, and 650 Rayleighs ± 10% observed by the high-resolution Fabry-Perot currently at Pine Bluff with a field of view of 1.4°. The atmospheric extinction coefficient (τ) is 0.078 at the Kitt Peak Observatory (WHAM) and 0.14 at the Pine Bluff Observatory (pre-WHAM).

[29] A composite of calibration observations of the North American Nebula was used to determine a clear sky calibration factor for each yearly season of WHAM observations. Monitoring of the nebular calibration spectra enabled us to track annual changes in the sensitivity of the WHAM instrument. The NAN observations used to calibrate the WHAM geocoronal observations were limited to observations taken at zenith angles less than or equal to 50° to minimize the effects of atmospheric extinction along the observational slant path.

[30] To track changes in the calibration associated with changes in the sensitivity of the Wisconsin H-α Mapper Fabry-Perot over the time span of the WHAM solar cycle 23 study, we used a calibration factor, F_{NAN}, defined as follows.

$$F_{NAN} = \frac{A_{NAN}}{\{I_{NAN}[\exp(-\tau \sec ZA_{NAN})][\text{exposure time}(NAN)]\}} \quad (2)$$

This calibration factor (F_{NAN}) has units of $\frac{[\text{Adu (arbitrary data units)}]\left[\frac{\text{km}}{\text{sec}}\right]}{\text{Rayleighs} \times \text{sec}}$. Table 1 contains calibration factors obtained for the years of WHAM observations included in this paper. We also include the number of top quality observations of the North American Nebula used to calculate each year's factor.

[31] We used observations of the North American Nebula taken during northern hemisphere spring/summer and fall because during these months the nebula is visible at zenith angles of less than 50°. During winter months, NAN is not visible in this range of zenith angles. To calculate the calibration factor, we used an average calculated from NAN observations taken during the previous fall and during the spring/summer period subsequent to the winter observations. Calibration factors derived from the individual NAN observations used to determine each annual calibration factor differed by less than 3% from the average value, reflecting the uncertainty in the relative calibration due to night-to-night variability in atmospheric transmission. The calibration factors in Table 1 above are consistent with the current WHAM calibration value used by the WHAM astronomers of 22.8 Adu km sec^{-2} Rayleighs^{-1}, which is often sited as 684.1 Adu km sec^{-1} Rayleighs^{-1} for a 30 second exposure [*Haffner et al.*, 2003]. The WHAM instrument began observations at Kitt Peak in 1997 and experienced a decrease in sensitivity, probably after the dust settled in the instrument. The decrease in calibration factor, F_{NAN}, reflects this decrease in instrumental sensitivity.

[32] The North American Nebula has been calibrated using standard stars [*Scherb*, 1981] and has also been checked against a blackbody source [*Nossal*, 1994]. The accuracy of this calibration has also been corroborated with a comparison to the Southern H-α Sky Survey Atlas [*Gaustad et al.*, 2001].

5. Solar Cycle 23 WHAM Observations

[33] A sample WHAM Balmer α spectrum in a region of very low Galactic emission (0.20 Rayleighs) is displayed in Figure 2b. The observation was from 13 March 1997 and is included in the solar cycle plot of Figure 3. The exposure time for the observation was 30 seconds. Spectral displacement is expressed in velocity units with an arbitrary "zero" velocity. The centroid of the fine structure (two-component) fit to the geocoronal line is located at 96.8 km/s and its intensity is 4.1 Rayleighs (see Figure 2b). The fit includes the Galactic emission (0.20 Rayleighs) at 105 km/s and a faint O_2 band atmospheric emission (0.13 Rayleighs) at 57.5 km/s [*Nossal et al.*, 2004; *Hausen et al.*, 2002]. The retrieved geocoronal intensities also include the cascade excitation which is estimated to be 5 ± 3% of the total intensity (see, for example, *Mierkiewicz et al.* [2006] and *Meier* [1995]). For this example of maximum overlap between the geocoronal and Galactic emissions, the retrieved geocoronal intensity differed by 2.8% when the Galactic emission was not explicitly included in the fit, as was the case for the WHAM solar cycle observations taken in low Galactic emission directions. The uncertainty in the fit to the geocoronal intensity is 0.2% based on scatter in the data.

[34] Figure 3 displays solar cycle 23 WHAM thermospheric plus exospheric Balmer α column emission observations plotted versus shadow altitude. These observations are primary measurements, uncorrected for tropospheric scattering. The observations of Figure 3 were taken between December and the Spring equinox when sky conditions are typically better and nights longer. We have historically seen reproducibility in our measurements within a given dark of the moon observing period.

[35] The observations included on this plot were limited to those pointed in very low Galactic emission regions of the celestial sky [*Hausen et al.*, 2002; *Nossal et al.*, 2004]. Most were taken in directions where the Galactic emission was less than 0.3 Rayleighs. Some were taken in directions with up to 0.6 Rayleighs of Galactic emission, but where the Doppler shift between the emissions was more than 13 km/sec, resulting in little overlap between the two emissions. Regions of low Galactic emissions are monitored as reference directions on most nights of WHAM observations. The 1997 solar minimum data [F10.7 (solar flux index) 69–76; Ap (geomagnetic index) 2–9 with one day having an Ap of 22] are from 10 nights of observations, the 2004 solar medium data (F10.7 100–118; Ap 3–15) are from five nights of observations, the 2000 and 2001 near solar maximum data (F10.7 134–163; Ap 4–11) are from eight nights of observations, and the 2006 solar minimum data (F10.7 75–77; Ap 2–4) are taken from two nights of observations.

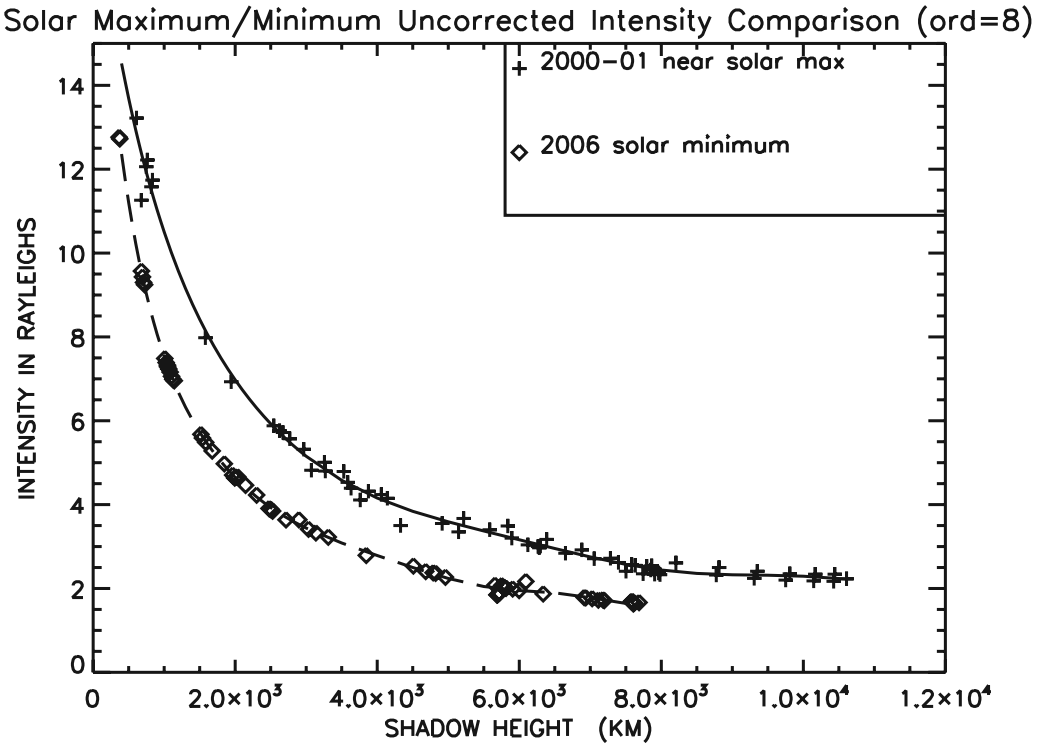

Figure 4. Eighth-order polynomial fit to the 2000 and 2001, and to the 2006 observations of Figure 3.

[36] We observe higher column emission intensities during near-solar maximum periods with the ratio dependent upon viewing geometry. For example, at the midrange shadow altitude of 3000 km, WHAM geocoronal H-α column emission intensities are a factor of about 1.5 higher during near solar maximum conditions than during solar

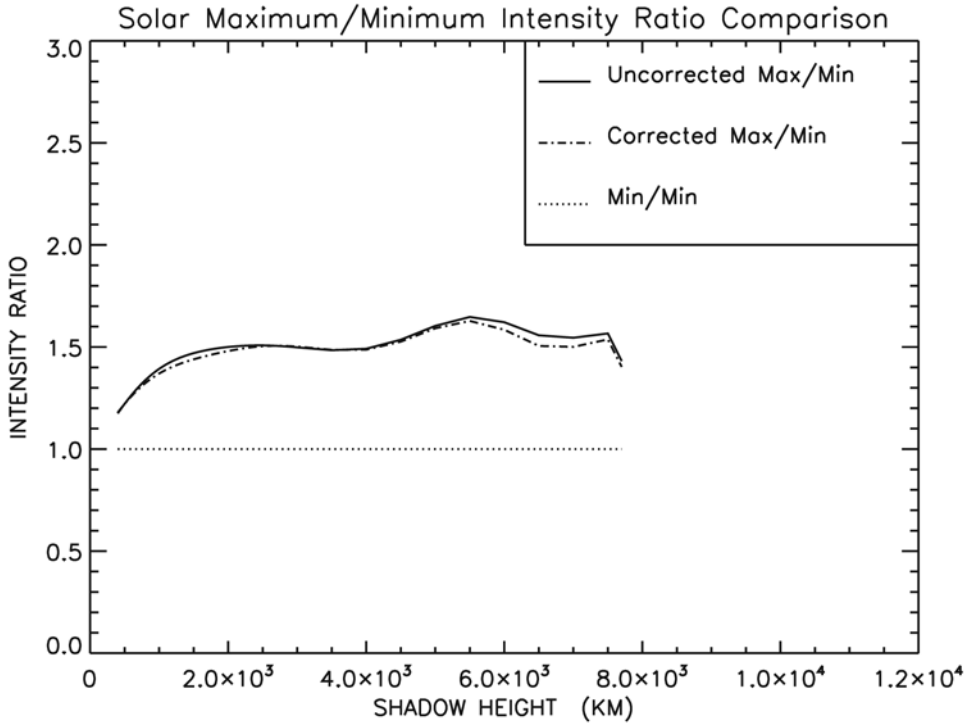

Figure 5. The polynomial fits for the years 2000 and 2001, and for the 2006 observations (see Figure 4) are taken in ratio to the 2006 polynomial fit (solid line). The ratio when the data are corrected for tropospheric scattering using the correction code of *Leen* [1979] (dash-dotted line) is also included.

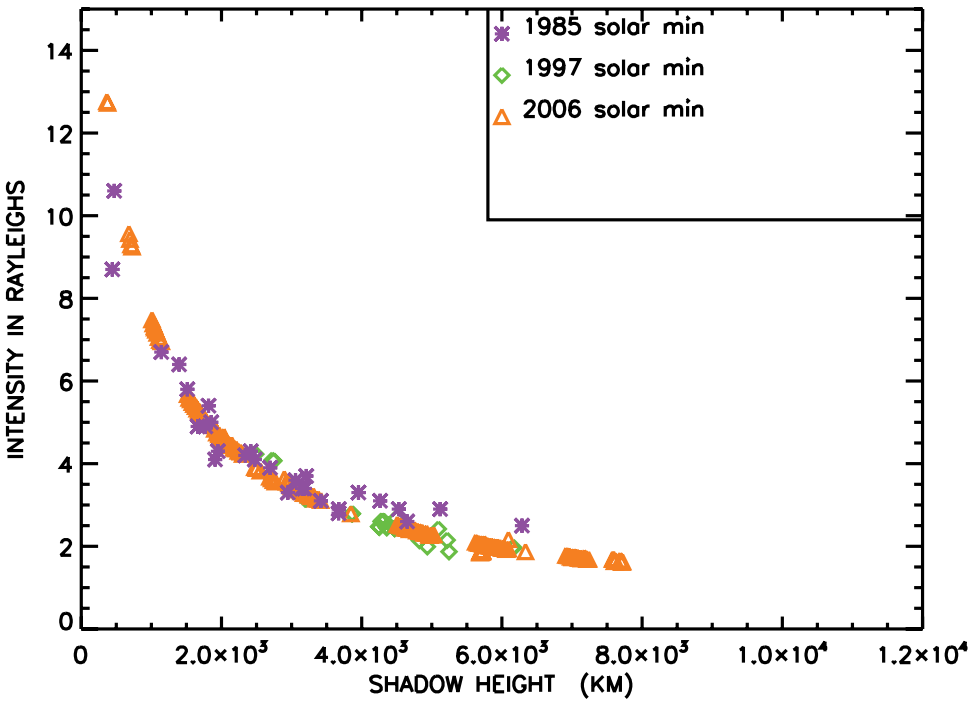

Figure 6. Comparison between midlatitude observations taken under solar minimum conditions during winter months by the Wisconsin H-α Mapper Fabry-Perot (Kitt Peak, Arizona) during 1997 and 2006 and throughout the year by a similarly designed double-etalon Fabry-Perot at Pine Bluff, Wisconsin in 1985. The observations of Figure 6 are the primary measurements. The uncertainty in the relative comparisons between WHAM and pre-WHAM observations is ~18% (see text).

minimum conditions (see Figures 3–5). The column emission intensities of the solar medium observations fall between those of the solar minimum and near maximum observations. The 2006 solar minimum intensities are again lower, in agreement with the 1997 solar minimum intensities.

[37] In Figure 4, an eighth-order polynomial has been fit to the 2000 and 2001 near solar maximum and 2006 solar minimum observations of Figure 3 to facilitate ratio comparisons between solar maximum and minimum observations. The 2000–2001and 2006 polynomial fits are then both taken in ratio to the 2006 polynomial fit and displayed in Figure 5. The ratio between solar maximum and minimum column emission intensities is close to 1.5 for both cases when the data are the uncorrected primary measurements and when they have been corrected for tropospheric scattering using the code of *Leen* [1979] [see also *Shih et al.*, 1985]. This code is a single scattering approximation based on Rayleigh scattering by molecules, Mie scattering by aerosols, and a small amount of absorption by ozone. The higher ratios at large shadow altitudes may be due to the magnification of small differences when ratios are taken between small numbers, or could be a real effect, not yet determined, of different hydrogen distributions and/or multiple scattering contributions at solar maximum and minimum. We have also examined the data for zenith angle dependence and found that the zenith angle does not significantly affect the ratio between the solar maximum and minimum WHAM observations.

[38] Dawn geocoronal Balmer α emission intensities have been observed at midlatitudes to be about 20% higher than those at dusk for shadow altitudes less than about 2000 km, with little difference for higher shadow altitudes [*Mierkiewicz et al.*, 2006]. This AM/PM asymmetry does not affect the ratio between the solar maximum and minimum intensities illustrated in Figures 4 and 5 because the observations at shadow altitudes below about 2000 km were all taken during morning hours. The observations in directions of very low Galactic emission included in this study are visible at low shadow altitudes only during morning hours during winter months at midlatitudes. Observations in Figures 4 and 5 at shadow altitudes above about 2000 km included both morning and evening observations that at this mid to high shadow altitude range do not show an AM/PM asymmetry.

6. Observations From Three Solar Minima

[39] Figure 6 displays observations taken under solar minimum conditions at midlatitudes during three subsequent solar minima. The 1997 and 2006 observations are taken toward very low Galactic emission regions by WHAM from Kitt Peak. The WHAM observations are compared with observations taken in 1985 by the "pre-WHAM" Fabry-Perot, then located at Pine Bluff.

[40] The "pre-WHAM" instrument used the current WHAM etalons in a scanning mode with photomultiplier detection. The intensities included are from an archive of intensities and are from observations taken throughout the year. The observations are not restricted to low Galactic emission directions, but the geocoronal and Galactic emissions either are separated by a large Doppler shift, or the Galactic emission was fit and removed from the geocoronal

emission (J. Harlander, personal communication, 2008). As in the case of the WHAM data, the emission model was convolved with an instrumental profile and fit to the observational spectra. Like the WHAM observations, the 1985 observations included in the solar minimum study were limited to those taken at zenith angles less than or equal to 50°.

[41] Solar minimum conditions are generally more similar from cycle to cycle than are conditions during solar maximum periods as indicated by the F10.7 flux. The F10.7 and Ap indices ranged respectively from 69–76 and from 2–9 (with one day having an Ap) during the 10 nights of 1997 observations and from 75–77 and 2–4 during the two nights of 2006 observations. The 1985 observations were taken on 10 nights throughout the year during which the F10.7 index ranged from 67–76 and the Ap index ranged from 4–33.

[42] There is agreement between solar minimum column emission intensity observations taken in 1985 from Wisconsin with the WHAM solar minimum observations taken in 1997 and 2006 from Kitt Peak, Arizona to within 15% over most of the shadow altitude range. This agreement is within the relative uncertainty associated with comparisons between observations taken by the WHAM and pre-WHAM instruments.

7. Comments on Observational Uncertainties

[43] The observational comparison presented here with the smallest uncertainty is the relative comparison between WHAM observations. The uncertainty in the absolute intensity calibration is ±10%, but this systematic error is a scaling factor for all of the WHAM data, and does not affect the relative comparisons between WHAM observations. There is a ±3–5% uncertainty in the WHAM relative intensity calibration for a given year due to differences in atmospheric transmission on a clear night. The inclusion of the Galactic emission in the spectral fits for very low Galactic emission directions produces an upper boundary ∼4% uncertainty in the retrieved geocoronal emission intensity [*Nossal et al.*, 2004], but a smaller contribution to the relative uncertainty for comparisons of observations pointed toward low Galactic emission regions of the sky. The fit uncertainty associated with the *Voigt-fit* two component fine structure fit to the WHAM spectra taken toward low Galactic emission region directions is less than 1%.

[44] When comparing the WHAM and pre-WHAM observations with one another, the uncertainty in the relative intensity calibration may be as much as 10% due to the different calibrations for the different fields of view of the two instruments. The higher atmospheric extinction coefficient for the Pine Bluff observing site produces more scatter in the pre-WHAM data than for the data at the high-altitude Kitt Peak Observatory.

[45] Another important factor contributing to uncertainty in the retrieved geocoronal Balmer α column emission intensity is the scattering in the troposphere of Balmer α photons from outside the field of view into the observational line of sight. When corrections are made to the WHAM solar cycle data using the tropospheric scattering code of *Leen* [1979] [see also *Shih et al.*, 1985], the solar cycle difference persists because the corrections are applied to both solar minimum and maximum conditions (see Figure 5). Depending on viewing geometry, for the data presented here the *Leen* code calculates that 9–20% of the *absolute* column emission intensity is due to tropospheric scattering. Because of the WHAM low Galactic emission observations being taken in similar viewing geometries, the *relative* difference in the tropospheric scattering contribution to the Balmer α column emission intensity calculated by the *Leen* code between the solar minimum and maximum observations is within 5% for like shadow altitudes.

[46] An additional source of uncertainty is the cascade emission that arises because of the excitation of higher energy states in the hydrogen atom by solar Lyman photons with energies higher than Lyman β. Cascading electrons from these higher energy excited states populate all of the $n = 3$ levels, producing emission from all seven Balmer α fine structure pathways. The cascade emission has been measured at solar maximum to be 5 ± 3% of the total geocoronal Balmer α emission [*Mierkiewicz et al.*, 2006; *Nossal et al.*, 1998]. Meier has calculated the cascade contribution to be ∼4% using high-resolution solar Lyman line observations from SOHO taken during solar minimum conditions [*Meier*, 1995; R. R. Meier, personal communication, 2005]. The difference between the cascade emission during solar minimum and maximum conditions is not definitively known, but is unlikely to be more than a few percent, on the basis of the measured and calculated values of the cascade emission.

[47] In summary, an upper boundary on the *relative* uncertainty associated with comparisons of WHAM observations of the Balmer α column emission intensity toward low Galactic emission regions is approximately 9.6%. This value is derived from a compilation of uncertainty factors for *relative* intensity comparisons (equation (3)).

$$UN_{\text{WHAM relative intensity}} = \sqrt{UN_{AT}^2 + UN_{GAL}^2 + UN_{FIT}^2 + UN_{TS}^2 + UN_{CAS}^2} \quad (3)$$

For WHAM, the relative uncertainty in the atmospheric transmission (UN_{AT}) is 0.05, in the inclusion of the Galactic emission in low Galactic emission directions (UN_{GAL}) is 0.04, in the spectral fit (UN_{FIT}) is 0.01, in the relative difference in tropospheric scattering between the solar maximum and minimum data (UN_{TS}) is 0.05, and in the difference in cascade contribution between solar maximum and minimum data (UN_{CAS}) is 0.05. Combining these uncertainty factors results in a value of 0.096 for the uncertainty in the relative intensity for WHAM data comparisons in observational directions pointed in directions toward low Galactic emission regions.

[48] An estimate for the *relative* uncertainty associated with comparisons between observations taken by the WHAM and pre-WHAM instruments (equation (4)) includes the added uncertainty associated with using absolute intensity calibrations for different fields of view.

$$UN_{\text{WHAM/Pre–WHAM relative intensity}} = \sqrt{UN_{\text{WHAM relative intensity}}^2 + UN_{CAL}^2 + UN_{pre-WHAM}^2} \quad (4)$$

As calculated above, the uncertainty in the WHAM relative intensity ($UN_{WHAM\ relative\ intensity}$) is 0.096. The uncertainty in the relative intensity calibration between the two fields of view for the WHAM and pre-WHAM instruments (UN_{CAL}) is ~0.10, and the additional uncertainty in the relative intensity calibration of the pre-WHAM instrument due to differences in atmospheric transmission, the Galactic emission, and fits to the data ($UN_{pre\text{-}WHAM}$) is ~0.12. Combining these uncertainty factors results in a value of 0.18 for the uncertainty in the relative comparisons between observations taken by the pre-WHAM and WHAM instruments.

[49] The factor of 1.5 difference between the WHAM observations of the Balmer α column emission intensity during solar maximum compared with solar minimum conditions over solar cycle 23 is statistically significant and greater in magnitude than the sources of relative error in the measurements (Figure 3). Additional error is associated with comparing observations from the WHAM instrument with those from the Pine Bluff "pre-WHAM" Fabry-Perot. Any variations in the observed Balmer α column emission intensities over three solar minima (1985, 1997, 2006) (see Figure 6) are within the estimated uncertainties associated with the relative comparison between observations taken by the WHAM and pre-WHAM instruments.

8. Discussion

[50] The higher signal-to-noise WHAM observations corroborate suggestions of a solar cycle trend in the Balmer α emission seen in Wisconsin observations taken over the previous solar cycle. These solar cycle 22 observations also measured higher geocoronal Balmer α intensities during solar maximum periods; however, past data were deemed to be of insufficient precision to make the variation statistically significant [*Nossal et al.*, 1993].

[51] Like our observations, the *Anderson et al.* [1987] model predicts higher geocoronal Balmer α column emission intensities from the ground-based observations during solar maximum conditions than during solar minimum conditions. The magnitude of the difference is dependent upon viewing geometry. Anderson et al. used Monte Carlo models of geocoronal hydrogen distributions as input to a radiative transfer model to predict geocoronal emission intensities that would be observed from a ground-based observatory [*Anderson et al.*, 1987]. The higher column emission intensities during solar maximum conditions result from the observations being an integrated column of emissions along a line of sight, the influence of escape processes, and that the Lyman β solar flux that excites the geocoronal hydrogen atoms is larger during solar maximum conditions. The *Anderson et al.* [1987] study used a solar Lyman beta excitation flux of 3, 5, and 9×10^9 photons $cm^{-2}\ s^{-1}\ A^{-1}$ for solar minimum, medium, and maximum conditions, respectively.

[52] The magnitude of the solar cycle difference predicted by *Anderson et al.* [1987] is greater than that of our observations. For example, at a midrange shadow altitude of about 3,000 km (~45° solar depression angle for zenith observations), the Anderson et al. model predicts that the column emission intensity is a factor of about 2.4 times greater at solar maximum than at solar minimum. Recent measurements by the SOHO instruments indicate that the solar Lyman beta flux at solar minimum is more likely to be closer to 5×10^9 photons $cm^{-2}\ s^{-1}\ A^{-1}$ rather than the near solar minimum value of 3×10^9 photons $cm^{-2}\ s^{-1}\ A^{-1}$, used by *Anderson et al.* [1987] [*Bishop et al.*, 2001; *Warren et al.*, 1998]. Scaling the *Anderson et al.* [1987] midrange column emission intensities by the revised solar minimum flux results in a difference of about a factor of 1.4 between the predicted higher solar maximum intensities and the lower solar minimum intensities. This prediction is in the same direction and closer in magnitude to the difference of about 1.5 in the Balmer α column emission intensity that the WHAM instrument has observed between solar maximum and solar minimum for midrange shadow altitudes (see Figures 3–5).

[53] The WHAM observations are in agreement with trends predicted by the *Anderson et al.* [1987] model of higher ratios from solar maximum to minimum for the Balmer α column emission intensity at high shadow altitudes. Multiple scattering is a larger percentage of the signal at high shadow altitudes. This factor along with solar cyclic differences in the hydrogen density profile may contribute to the higher maximum/minimum intensity ratios at higher shadow altitudes.

[54] There is agreement between solar minimum column emission intensity observations taken in 1985 from Wisconsin and in 1997 and 2006 from Kitt Peak, Arizona over most of the shadow altitude range to within 18% uncertainties. R.J. Reynolds has preserved original spectra from the 1970s and 1980s (R.J. Reynolds, personal communication, 2008). We anticipate that the scatter in the 1985 observations will likely be reduced following planned reanalysis with modern techniques and improved knowledge of the Galactic emission from WHAM. In addition, the uncertainties in the relative comparisons of WHAM and pre-WHAM observations could be reduced in the future with the use of an improved tropospheric scattering correction code, accounting for current knowledge of tropospheric constituent profiles of major species involved in scattering. In particular, improved tropospheric scattering corrections may help to interpret the slightly higher intensities observed at high shadow heights from Pine Bluff, Wisconsin, than at the Kitt Peak Observatory site (see Figures 1 and 6).

[55] Long-term geocoronal Balmer α data sets have also been acquired by observers at the Arecibo Observatory (see, for example, *Atreya et al.* [1975], *Meriwether et al.* [1980], *He et al.* [1993], *Kerr et al.* [2001a, 2001b, and references therein]) and at the Abastumani Observatory, near Tiblisi Georgia [*Martsvaladze and Fishkova*, 1991]. Observers from the lower latitude Arecibo Observatory reported an opposite solar cyclic dependence in their observations with higher intensities during solar minimum than during solar maximum conditions for shadow altitudes less than about 2000 km, [*Kerr et al.*, 2001a], in contrast to the higher intensities observed during solar maximum periods at Wisconsin and Arizona. These differences have not yet been understood. Intercomparison of these data sets with the Wisconsin long-term record will require review of data acquisition and analysis techniques for the three sites, including viewing geometry and the Galactic emission.

[56] Now that our data are of sufficient extent and precision to investigate solar cycle trends and to begin to examine possible climatic signatures in our geocoronal hydrogen observations, further modeling studies are needed to predict the magnitude of expected trends over the time span of the Wisconsin midlatitude data record. *Qian et al.*

[2006] used historical time-dependent values for solar UV fluxes [*Solomon and Qian*, 2005] and lower boundary carbon dioxide concentrations in a single column version of the NCAR/TIMEGCM (National Center for Atmospheric Research/Thermosphere Ionosphere Mesosphere Electrodynamics General Circulation Model) [*Roble et al.*, 1987; *Roble and Dickinson*, 1989] to investigate the upper atmosphere's response to the solar cycle and to increases in carbon dioxide radiative cooling to space. The *Qian et al.* [2006] study found that thermospheric density decreases because of upper atmospheric cooling were about three times larger in magnitude during solar minimum conditions compared with solar maximum conditions. Similarly, further modeling with historical values of methane, as well as carbon dioxide and solar fluxes will be required to better understand the magnitude of any predicted solar cyclic and climatic changes in hydrogen and whether climatic changes are more pronounced during particular phases of the solar cycle.

[57] Geocoronal hydrogen column emission observations are a function of both the altitude profile of hydrogen and the incoming solar UV radiation, both of which change over the course of the solar cycle. Multiple scattering of solar Lyman line radiation below the Earth's shadow complicates the analysis of the observations. Thus detailed data/forward modeling comparisons with a code such as the *LYAO_RT* global resonance radiative transfer code [*Bishop*, 1991, 1999, 2001; *Bishop et al.*, 2001, 2004] is required to facilitate comparison between model predictions of hydrogen densities and our observations.

[58] The Wisconsin long-term geocoronal hydrogen emission data set has quantified evidence for a statistically significant solar cyclic response in the hydrogen Balmer α column emission with higher intensities observed during solar maximum conditions. There is agreement in observations taken during three solar minima periods, 1985, 1997, and 2006 to within uncertainties. Continued high signal-to-noise observations, along with careful accounting for calibration and data quality factors can assist in the acquisition of longer time data records in the upper atmosphere and the comparison of these with future observations.

[59] **Acknowledgments.** The authors thank Greg Madsen, Nicole Hausen, Steve Tufte, and Robert Benjamin for sharing observations that they took using the Wisconsin H-α Mapper Fabry-Perot. We are very grateful for our many years of collaboration with the late James Bishop and his invaluable insights regarding geocoronal science. We thank Jeff Percival for assistance with the development of analysis codes for calculating the shadow altitude. Barbara Emery's helpful discussions regarding the documentation of our observations and analysis methods for the CEDAR database have contributed to the presentation of topics included in this paper, particularly the calibration section. Liying Qian, Stan Solomon, and Ray Roble have provided valuable guidance regarding NCAR models. We also thank John Harlander, Frank Scherb, Monica Coakley, Peifu Shih, and Roger Yelle for their contributions to the Wisconsin geocoronal research program. We thank both reviewers for their careful reading and thoughtful comments that greatly assisted us in improving the paper. This research was supported by the National Science Foundation grants ATM-0334611 and AST-9619424.

[60] Wolfgang Baumjohann thanks Kazuo Shiokawa and Robert Kerr for their assistance in evaluating this paper.

References

Anderson, D. E., Jr., R. R. Meier, R. R. Hodges Jr., and B. A. Tinsley (1987), Hydrogen Balmer alpha intensity distributions and line profiles from multiple scattering theory using realistic geocoronal models, *J. Geophys. Res.*, *92*(A7), 7619–7642.

Atreya, S. K., P. B. Hayes, and A. F. Nagy (1975), Doppler profile measurements of the geocoronal hydrogen Balmer alpha line, *J. Geophys. Res.*, *80*(4), 635–638.

Bishop, J. (1991), Analytic exosphere models for geocoronal applications, *Planet. Space Sci.*, *39*, 885–893.

Bishop, J. (1999), Transport of resonant atomic hydrogen emissions in the thermosphere and geocorona: Model descriptions and applications, *J. Quant. Spectrosc. Radiat. Transfer*, *61*, 473–491.

Bishop, J. (2001), Thermospheric atomic hydrogen densities and fluxes from dayside Lyman α measurements, *J. Atmos. Sol.-Terr. Phys.*, *63*, 331–340.

Bishop, J., J. Harlander, S. Nossal, and F. L. Roesler (2001), Analysis of Balmer α intensity measurements near solar minimum, *J. Atmos. Sol.-Terr. Phys.*, *63*, 341–353.

Bishop, J., E. J. Mierkiewicz, F. L. Roesler, J. F. Gomez, and C. Morales (2004), Data- model comparison search analysis of coincident PBO Balmer α, EURD Lyman β geocoronal measurements from March 2000, *J. Geophys. Res.*, *109*, A05307, doi:10.1029/2003JA010165.

Brasseur, G., and S. Solomon (2005), *Aeronomy of the Middle Atmosphere*, Springer, New York.

Chamberlin, J. W., and D. M. Hunten (1987), *Theory of Planetary Atmospheres: An Introduction to their Physics and Chemistry*, 2nd ed., Elsevier, New York.

Coakley, M. M., F. L. Roesler, R. J. Reynolds, and S. Nossal (1996), Fabry-Perot/CCD annular summing spectroscopy: Study and implementation for aeronomy applications, *Appl. Opt.*, *35*, 6479–6493.

Ehhalt, D. H. (1986), On the consequence of tropospheric CH4 increase to the exospheric density, *J. Geophys. Res.*, *91*(D2), 2843–2843.

Garcia, R. R., D. R. Marsh, D. E. Kinnison, B. A. Boville, and F. Sassi (2007), Simulation of secular trends in the middle atmosphere, 1950–2003, *J. Geophys. Res.*, *112*, D09301, doi:10.1029/2006JD007485.

Gaustad, J. E., P. R. McCullough, W. Rosing, and D. VanBuren (2001), A robotic wide-angle H-alpha survey of the southern sky, *Publ. Astron. Soc. Pac.*, *113*, 1326.

Haffner, L. M., R. J. Reynolds, S. L. Tufte, G. J. Madsen, K. P. Jaehnig, and J. W. Percival (2003), The Wisconsin H-alpha mapper northern sky survey, *Astrophys. J.*, *149*, 405–422.

Hausen, N. R., R. J. Reynolds, L. M. Haffner, and S. L. Tufte (2002), Interstellar Hα line profiles toward HD 93521 and the Lockman window, *Astrophys. J.*, *565*, 1060–1068.

He, X., R. B. Kerr, J. Bishop, and C. A. Tepley (1993), Determining exospheric hydrogen density by reconciliation of Hα measurements with radiative transfer theory, *J. Geophys. Res.*, *98*(A12), 21,611–21,626.

Kerr, R. B., et al. (2001a), Periodic variations of geocoronal Balmer α brightness due to solar driven exospheric abundance variations, *J. Geophys. Res.*, *106*(A12), 28,797–28,817.

Kerr, R. B., et al. (2001b), Secular variability of the geocoronal Balmer α brightness: Magnetic activity and possible human influences, *J. Geophys. Res.*, *106*(A12), 28,819–28,829.

Leen, T. (1979), Application of radiative transfer theory to photometric studies of astronomical objects, M.S. thesis, Univ. of Wis., Madison, Wis.

Martsvaladze, N. M., and L. M. Fishkova (1991), Radiation of the upper atmosphere and geocoronal hydrogen in 1958–1988 on observation of the HI 656.3nm emission in Abastumani, *Geomagn. Aeron.*, *31*(6), 1017–1020.

Meier, R. R. (1995), Solar Lyman-series line profiles and atomic hydrogen excitation rates, *Astrophys. J.*, *452*, 462–471.

Meriwether, J. W., Jr., S. K. Atreya, T. M. Donahue, and R. G. Burnside (1980), Measurements of the spectral profile of Balmer alpha emission from the hydrogen geocorona, *Geophys. Res. Lett.*, *7*(11), 967–970.

Mierkiewicz, E. J. (2002), Fabry-Perot observations of the hydrogen geocorona, Ph.D. thesis, Univ. of Wis., Madison, Wis.

Mierkiewicz, E. J., F. L. Roesler, S. M. Nossal, J. Bishop, R. J. Reynolds, and L. M. Haffner (2006), Geocoronal hydrogen studies using Fabry-Perot Interferometers. part 1: instrumentation, observations, and analysis, *J. Atmos. Sol.-Terr. Phys.*, *68*, 1520–1552, doi:10.1016/j.jastp. 2005. 08.024.

Nossal, S. (1994), Fabry-Perot observations of geocoronal hydrogen Balmer-alpha emissions, Ph.D. thesis, Univ. of Wis., Madison, Wis.

Nossal, S., F. L. Roesler, and M. M. Coakley (1998), Cascade excitation in the Geocoronal hydrogen Balmer-α line, *J. Geophys. Res.*, *103*(A1), 381–390.

Nossal, S., R. J. Reynolds, F. L. Roesler, and F. Scherb (1993), Solar cycle variations of geocoronal Balmer α emission, *J. Geophys. Res.*, *98*(A3), 3669–3676.

Nossal, S., F. L. Roesler, R. J. Reynolds, M. Haffner, S. Tufte, J. Bishop, and J. Percival (2001), Geocoronal Balmer α intensity measurements using the WHAM Fabry-Perot facility, *J. Geophys. Res.*, *106*(A4), 5605–5616.

Nossal, S. M., F. L. Roesler, E. J. Mierkiewicz, and R. J. Reynolds (2004), Observations of solar cyclical variations in geocoronal Hα column emis-

sion intensities, *Geophys. Res. Lett.*, *31*, L06110, doi:10.1029/2003GL018729.

Nossal, S. M., E. J. Mierkiewicz, F. L. Roesler, R. J. Reynolds, and L. M. Haffner (2006), Geocoronal hydrogen studies using Fabry-Perot interferometers. part II: Long term observations, *J. Atmos. Sol. Terr. Phys.*, *68*, 1553–1575, doi:10.1016/j.jastp.2005.08.025.

Qian, L., R. G. Roble, S. C. Solomon, and T. J. Kane (2006), Calculated and observed climate change in the thermosphere, and a prediction for solar cycle 24, *Geophys. Res. Lett.*, *33*, L23705, doi:10.1029/2006GL027185.

Reynolds, R. J. (1984), A measurement of the hydrogen recombination rate in the diffuse interstellar medium, *Astrophys. J.*, *282*, 191.

Reynolds, R. J. (1997), Ionizing the galaxy, *Science*, *277*, 1446–1447.

Reynolds, R. J., F. L. Roesler, F. Scherb, and J. Harlander (1990), Fabry-Perot/CCD multi-channel spectrometer for the study of warm, ionized interstellar gas and extraGalactic clouds, in *Instrum. Astron. VII Proc. Int. Soc. Opt. Eng.*, *1235*, edited by D. Crawford, p. 610, SPIE, Washington.

Roble, R. G. (1995), Major Greenhouse cooling (yes cooling): The upper atmosphere response to increased CO_2, *Rev. Geophys.*, *33*(S1), 539–546.

Roble, R. G., and E. C. Ridley (1994), A thermosphere-ionosphere-mesosphere-electrodynamics general circulation model (time-GCM): Equinox solar cycle minimum simulations (30–500 km), *Geophys. Res. Lett.*, *21*(6), 417–420.

Roble, R. G., and R. E. Dickinson (1989), How will changes in carbon dioxide and methane modify the mean structure of the mesosphere and thermosphere?, *Geophys. Res. Lett.*, *16*(12), 1441–1444.

Roble, R. G., E. C. Ridley, and R. E. Dickinson (1987), On the global mean structure of the thermosphere, *J. Geophys. Res.*, *92*(A8), 8745–8758.

Roesler, F. L. (1974), Fabry-Perot instruments for astronomy, in *Methods of Experimental Physics*, vol. 12, Part A: Optical and Infrared, edited by M. Carlton, p. 531, Academic Press, New York.

Scherb, F. (1981), Hydrogen production rates from ground-based Fabry-Perot observations of comet Kohoutek, *Astrophys. J.*, *243*, 644.

Shih, P., F. L. Roesler, and F. Scherb (1985), Intensity variations of geocoronal Balmer alpha emission: 1. Observational results, *J. Geophys. Res.*, *90*(A1), 477–490.

Solomon, S. C., and L. Qian (2005), Solar extreme-ultraviolet irradiance for general circulation models, *J. Geophys. Res.*, *110*, A10306, doi:10.1029/2005JA011160.

Solomon, S., D. Qin, M. Manning, Z. Chen, M. Marquis, K. B. Averyt, M. Tignor, and H. L. Miller (Eds.) (2007), *Climate Change 2007: The Physical Science Basis. Contribution of Working Group I to the Fourth Assessment Report of the Intergovernmental Panel on Climate Change*, Cambridge Univ. Press, New York.

Trauger, J. T. (1976), Broadband dielectric mirror coatings for Fabry-Perot spectroscopy, *Appl. Opt.*, *15*, 2998–3005.

Warren, H. P., J. T. Mariska, and K. Wilhelm (1998), High-resolution observations of the solar hydrogen Lyman lines in the quiet sun with the SUMER instrument on SOHO, *Astrophys. J., Suppl. Ser.*, *119*, 105–120.

Yelle, R. V., and F. L. Roesler (1985), Geocoronal Balmer alpha line profiles and implications for the exosphere, *J. Geophys. Res.*, *90*(A8), 7568–7580.

L. M. Haffner and R. J. Reynolds, Department of Astronomy, University of Wisconsin-Madison, 475 N. Charter Street, Madison, WI 53706, USA.

E. J. Mierkiewicz, S. M. Nossal, and F. L. Roesler, Department of Physics, University of Wisconsin-Madison, 1150 University Avenue, Madison, WI 53706, USA. (nossal@physics.wisc.edu)

R. C. Woodward, Department of Computer Science, Engineering, Physics and Astronomy, University of Wisconsin-Fond du Lac, 400 University Drive, Fond du Lac, WI 54935, USA.